

# SR-WTA: Skyrmion Racing Winner-Takes-All Module for Spiking Neural Computing

Biao Pan<sup>\*</sup>, Kang Wang<sup>†</sup>, Xing Chen<sup>†</sup>, Jinyu Bai<sup>†</sup>, Jianlei Yang<sup>‡</sup>, Youguang Zhang<sup>\*</sup> and Weisheng Zhao<sup>†</sup>

Email: {mingren200323, wang.kang, xing.chen0118, 13021042, jianlei, zyg, weisheng.zhao}@buaa.edu.cn

<sup>\*</sup>School of Electronic and Information Engineering, Beihang University, Beijing 100191, China.

<sup>†</sup>School of Microelectronics, Beihang University, Beijing 100191, China.

<sup>‡</sup>School of Computer Science and Engineering, Beihang University, Beijing, 100191, China.

**Abstract**— Spiking neural network (SNN) has emerged as one of the popular architectures in complex pattern recognition and classification tasks. However, hardware implementation of such algorithms using conventional CMOS based neuron consume resources and power that are orders of magnitude higher than that in human brain. This can be attributed to the mismatch of the computational architecture between biological brain and the current Boolean logic computing platform. Magnetic skyrmions have been intensively studied as a prospective information carrier in neuromorphic computing hardware design. In this work, a compact time-domain skyrmion-racing winner-takes-all (SR-WTA) leaky-integrate-fire (LIF) spiking neuron network is presented for the first time. The skyrmion motion dynamics in the LIF neuron and the behaviors of the neuron network was investigated comprehensively. Both SPICE and micromagnetic simulations are performed to evaluate the functionality and performance of the proposed SR-WTA based SNN.

**Keywords**— Skyrmion, Spiking Neural Network, SR-WTA, LIF neuron, Bio-inspired.

## I. INTRODUCTION

Neural networks have been widely adopted for a range of classification and recognition applications due to their superior performances over traditional machine learning algorithms [1-6]. In order to effectively implement a neuron network in hardware, artificial neurons with ideal energy performance are essential [7-9]. In the last decades, the leaky-integrate-fire (LIF) neuron model originated from Hodgkin-Huxley model has attracted extensive attention for building bio-inspired spiking neuron network (SNN) [10]. Nevertheless, most reported LIF neurons still relies on semiconductor-based circuits via integrating transistors [11,12], greatly sacrificing integration density. Therefore, a compact and energy-efficient single-device implementation of LIF neuron is preferable for mimicking the biological neuron and the computing capacity be fully utilized.

Magnetic skyrmion are topologically stable spin configurations which can be stabilized by Dzyaloshinskii-Moriya interactions (DMI) in chiral bulk magnets or in thin films with broken inversion symmetry [13,14]. Owing to their ultra-small size (<10 nm), high drifting velocity (~75 m/s) with ultra-low depinning current density (~10<sup>6</sup> A/m<sup>2</sup>) and high defect tolerance [15], skyrmion have emerged as prospective information carriers in neuromorphic computing hardware design. Recent experiments have demonstrated the existence, stability, current-induced motion and detection of skyrmions at room temperature [16-18]. Meanwhile, a variety of skyrmion-based devices have been proposed. In particular,

several proposals attempt to employ skyrmions in neural networks: a skyrmion-based artificial synapse has been proposed in [19], in which both the short-term plasticity and long-term potentiation functionalities were demonstrated. Afterwards, skyrmion-based artificial neurons have also been designed in [20, 21], in which the neuronal activation function is achieved, mimicking the activity of a biologic neuron. These studies demonstrated the critical functions of skyrmion-based neurons and paved a new way for advanced neuromorphic computing applications such as pattern recognition. The intrinsic properties of skyrmions may enable us to build SNN with improved LIF neuron performance which is inaccessible to conventional electronic devices.

In this work, we propose a compact time-domain skyrmion-racing winner-takes-all (SR-WTA) neural network based on single-device leaky-integrate-fire (LIF) spiking neurons. The LIF spiking neuron exploits the tunable current-driven skyrmion motion dynamics along a nanotrack and translates the received spike current from other connected pre-neurons into the skyrmion racing velocity. A strong input spike current (amplitude or/and frequency) will lead to a fast skyrmion racing velocity. The skyrmion racing distance follows an “integrate-leaky” behavior depending on the temporal on/off duration of the input spike current pulse. Once the skyrmion reaches the finishing line (i.e. pre-defined threshold distance), it will be quickly detected and the neuron will “fire” an output spike and then reset. Only the first spiking neuron, in which the skyrmion first reaches the finishing line, will ever spike, (i.e. win over the others), by sharing a global reset signal for all the post-neurons via a feedback network. The skyrmion motion dynamics for the LIF artificial neuron and the WTA network are studied through micromagnetic and SPICE simulations, respectively. The rest of this paper is organized as follows: Section II discusses the background of the cortical LIF neuron model and skyrmion based neuron. Section III presents the proposed implementation of SR-WTA. In Section IV, micromagnetic and SPICE simulation methods are employed to carefully analyze the proposed SR-WTA SNN. Section V summarizes the work.

## II. BACKGROUND

### A. LIF neuron

In Fig. 1(a), we show a pair of biological neurons along with the interconnecting synapses. A form of sharp electrical pulses known as spikes are sent on a pre-neuron’s axon to the dendrites of post-neurons. The dendrites and axon blocks are implemented using interconnect circuits which model the spiking signal. Upon the reception of a particular spike, the membrane potential ( $V_{mem}$ ) of the associated neuron rises by

This work was supported by the China Postdoctoral Science Foundation (2018M640044) and the National Natural Science Foundation of China (61871008).

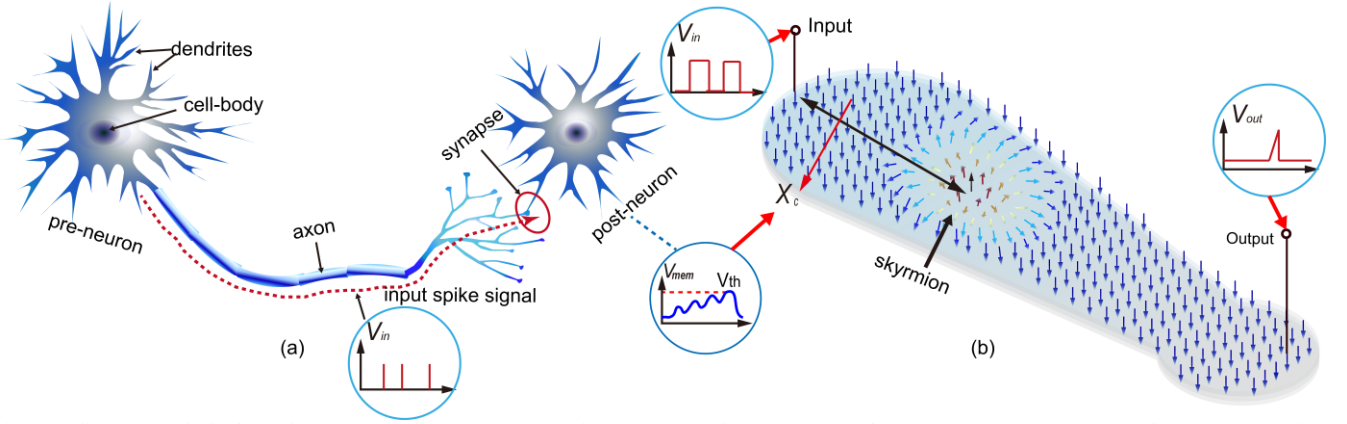


Fig.1 (a) Illustration of a biological LIF post-neuron receives inputs from pre-neuron by interconnected synapses. (b) A representative skyrmion neuron for accumulating inputs generated by different pre-neurons.

a certain amount and then decays slowly until the next spike is received. When the membrane potential exceeds a certain threshold, the associated neuron will emit a spike signal. Thus, the neuron exhibits the LIF dynamics, which is altered by the weights of the synaptic interconnections between the neurons. Once a neuron fires, it remains non-responsive for a certain period of time known as the refractory period [22].

This LIF neuron can be described by (1):

$$C_{mem} \frac{dV_{mem}}{dt} = -\frac{V_{mem}}{R_{mem}} + \sum_j \delta(t - t_j) w_j \quad (1)$$

where  $V_{mem}$  is the membrane potential,  $R_{mem}$  is the membrane resistance,  $C_{mem}$  is the membrane capacitance,  $w_j$  is the synaptic weight for the  $j$ -th input, and  $\delta(t - t_j)$  is the spiking event occurring at time instant  $t_j$ .

### B. Skyrmion Neuron

Correspondingly, the schematic diagram of the skyrmion neuron is shown in Fig.1(b). A skyrmion is initially nucleated at an origin position and then move forward along the nanotrack under the drive force of the accumulated spike current. During the movement, the skyrmion motion dynamics depends on the competition between the repulsive force from the nanotrack edge and the driving force of the accumulated input spike current, which depends then on the amplitude of the driving current [23]. The model of the skyrmion-based neuron is given as equation (2):

$$\tau_{mem} \frac{dV_{mem}}{dt} = -(V_{mem} - V_{reset}) + \sum_j \delta(t - t_j) w_j \quad (2)$$

where  $\tau_{mem}$  is the decay time constant,  $V_{mem}$  denotes the membrane potential (location of the skyrmion  $X_c$ ),  $V_{reset}$  is the resting potential,  $\sum_j \delta(t - t_j) w_j$  is the sum of the input weighted spikes from input terminal.

## III. PROPOSED IMPLEMENTATION

### A. Skyrmion Spiking Neuron Network Design

Fig. 2 illustrates the schematic of the proposed SR-WTA LIF spiking neuron network, which is composed of a set of LIF spiking neurons and WTA modules. The key component of the LIF spiking neuron is a synthetic antiferromagnetic exchange coupled bilayer nanotrack (see Fig. 2(b)), in which a skyrmion can move back and forth driven by an electrical

current pulse flowing through the heavy metal under the nanotrack via the spin Hall effect.

The nanotrack, which consists of a top ferromagnetic (FM) layer and a bottom FM layer separated by an insulating spacer layer, has a linear perpendicular magnetic anisotropy (PMA) to induce gradient anisotropy energy [21]. More importantly, this bilayer nanotrack supports two coupled skyrmions with opposite topological numbers in the top and bottom FM layers. In this configuration, the skyrmion Hall effect [23] can be completely suppressed owing to the cancellation of backaction forces acting on each individual skyrmion, resulting in a straight and fast motion of skyrmions along the current direction [24]. This property is essential in our design for ensuring the accurate translation between the intensity (amplitude or/and frequency) of the input spike current and the skyrmion racing distance.

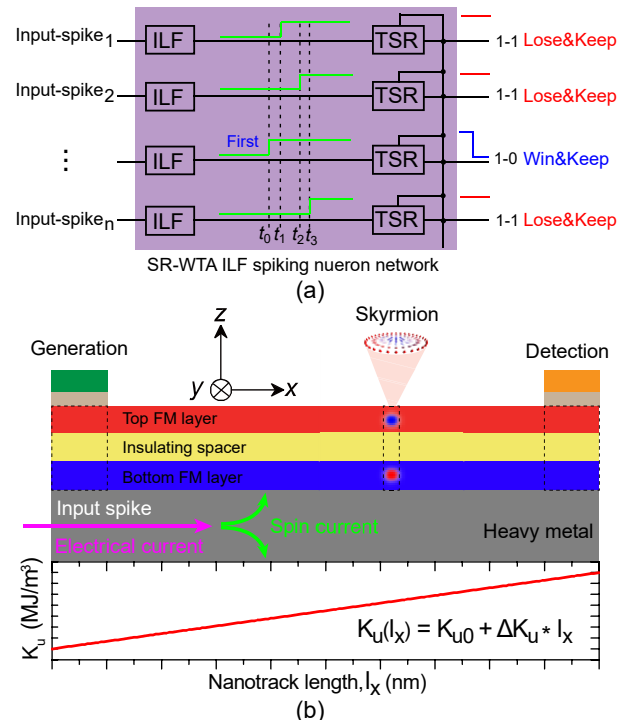


Fig. 2. Illustration of the proposed SR-WTA LIF spiking neuron network:(a) Overall schematic of the SR-WTA LIF spiking neuron network; (b) Schematic of the skyrmion-based single-device LIF artificial spiking neuron.

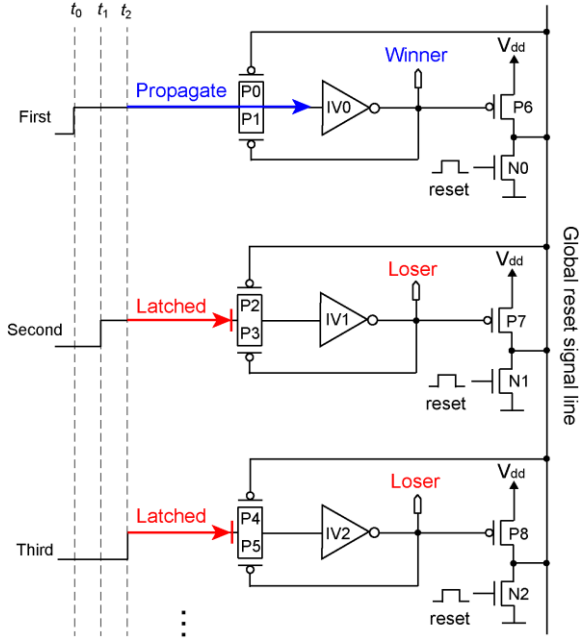


Fig. 3. Schematic of the TSR WTA circuit.

In addition, a skyrmion generation unit and a detection unit (e.g., spin-valve or magnetic tunnel junction [14, 25]) are placed at the two ends of the nanotrack, respectively. The received spike currents from other connected pre-neurons are utilized to drive the skyrmion motion along the nanotrack.

#### B. WTA Module

The WTA module consists of a set of trigger-suppression-reset (TSR) circuits sharing a global reset signal line, as shown in Fig. 3. Here for example, three skyrmion-racing spike signals from the pre-connected LIF artificial neurons arrive at time  $t_0$ ,  $t_1$  and  $t_2$ , respectively. In contrast to conventional WTA designs that decide the winner bit-by-bit or one-by-one, we only need to choose the first arrival spiking signal as the winner and shut off the others. The concept of the proposed WTA circuit is to use a pull-down switch to turn off the losers by activating a global reset signal line once the winner is detected. Initially, the global reset signal line is discharged to a low potential (Gnd) by turning on the NMOS transistors

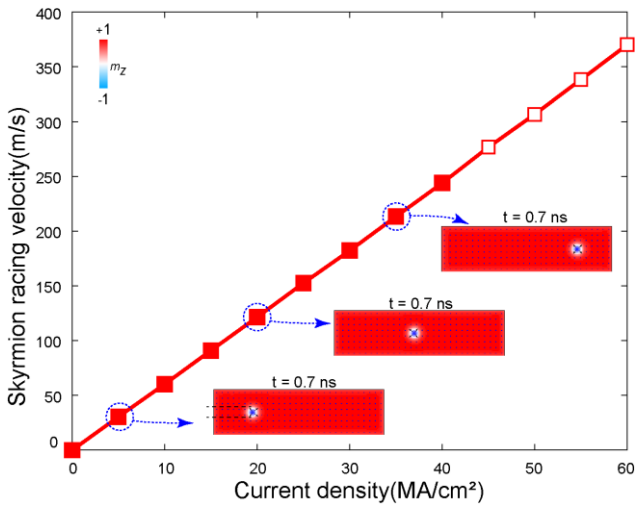


Fig. 4. Skyrmion racing velocity as function of input spike current density.

(N0-N2), which makes the PMOS transistors P0, P2, and P4 on, while P1, P3, and P5 off. Once the first neuron spikes, then the spiking signal will propagate forward to the inverter IV0 and makes the global reset signal line be pulled up to a high potential ( $V_{dd}$ ) by charging through P6. Meanwhile, P0, P2-P5 are turned off, making the other spiking signals from later spiking neurons disconnected from the TSR circuit. As can be seen, only the first spiking neuron will ever spike, i.e., win over the others.

#### IV. SIMULATION AND DISCUSSION

Our simulation framework consists of two main parts: (a) micromagnetic simulations for studying the skyrmion motion dynamics and for validating the functionality of the LIF spiking neuronal behavior; and (b) SPICE circuit simulations of the SR-WTA LIF spiking neuron network.

##### A. Micromagnetic Simulation

Micromagnetic simulations were performed using the Object Oriented Micro-Magnetic Framework (OOMMF) software [26] by solving the Landau-Lifshitz-Gilbert (LLG) equation including the DMI module [27] as (3).

$$\frac{dm}{dt} = -\gamma m \times h_{\text{eff}} + \alpha \left( m \times \frac{dm}{dt} \right) - \frac{\gamma \hbar P j_d}{2\mu_0 e M_s t_f} [m \times (m \times m_p)] \quad (3)$$

The key parameters summarized in Table.1 are as following: the width and length of the bilayer nanotrack are 80 nm and 300 nm, respectively, Gilbert damping  $\alpha = 0.3$ , exchange stiffness  $A = 15$  pJ/m, spin polarization  $P = 0.4$ , saturation magnetization  $M_s = 580$  kA/m, and DMI value  $D = 3$  mJ/m<sup>2</sup>. Furthermore, the PMA value of the nanotrack satisfies a linear relationship, i.e.,  $K_u(l_x) = K_{u0} + \Delta K_u \cdot l_x$ , in which  $K_{u0} = 0.7$  MJ/m<sup>3</sup>,  $\Delta K_u$  is the PMA increasing rate at  $7.0 \times 10^{-4}$  MJ/m<sup>3</sup> · nm, and  $l_x$  is the relative distance from the nanotrack origin. All samples are discretized into cells of  $2 \text{ nm} \times 2 \text{ nm} \times 1 \text{ nm}$  in the simulation, which is sufficiently smaller than the typical exchange length and the skyrmion size to ensure the numerical accuracy. More details on the micromagnetic simulations can refer to [14, 24]. The skyrmion racing velocity is linearly proportional to the density of the input spike current, as shown in Fig. 4. Therefore, the skyrmion racing velocity or distance can well correspond to the intensity of the input spike current. Initially, a skyrmion is generated under the generation unit. Then if any connected pre-neurons spike, the accumulated spike current drives the

TABLE. 1 KEY PARAMETERS IN SIMULATION.

Parameter	Description	Value
$M_s$	Sat. magnetization	580 kA/m
$A$	Exchange constant	15 pJ/m
$D$	DMI factor	3 mJ/m <sup>2</sup>
$\alpha$	Gilbert damping factor	0.3
$K_{u0}$	Magnetic anisotropy	0.7 MJ/m <sup>3</sup>
$P$	Spin polarization	0.4
$l \times w$	Length and width	300nm × 80nm

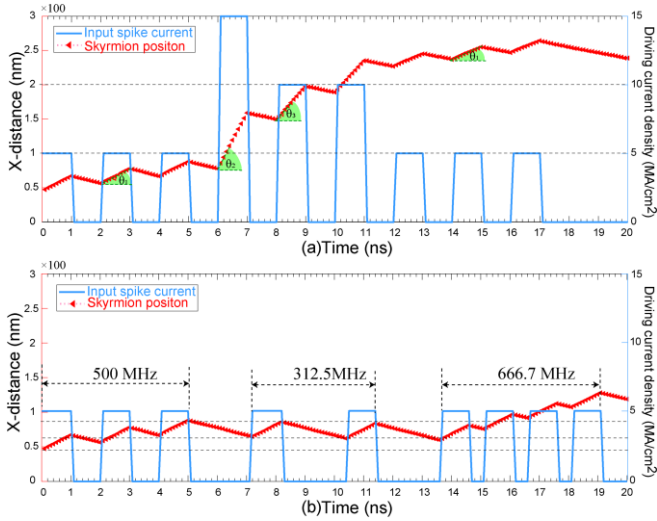


Fig. 5. Illustration of the skyrmion racing velocity (or distance) as a function of the density (a) and frequency (b) of the input spiking current, respectively. Here the X-distance to time (i.e., the slope angle  $\theta$ ) denotes the skyrmion racing velocity.

skyrmion racing along the nanotrack, depending on the competition between the gradient PMA energy and the driving force of the spike current pulse, which depends then on the intensity of the input spike current pulse.

The skyrmion racing distance exhibits an “integrate-leaky” behavior, as shown in Fig. 5, mimicking the membrane potential of a biological neuron. Fig. 5 illustrates the skyrmion

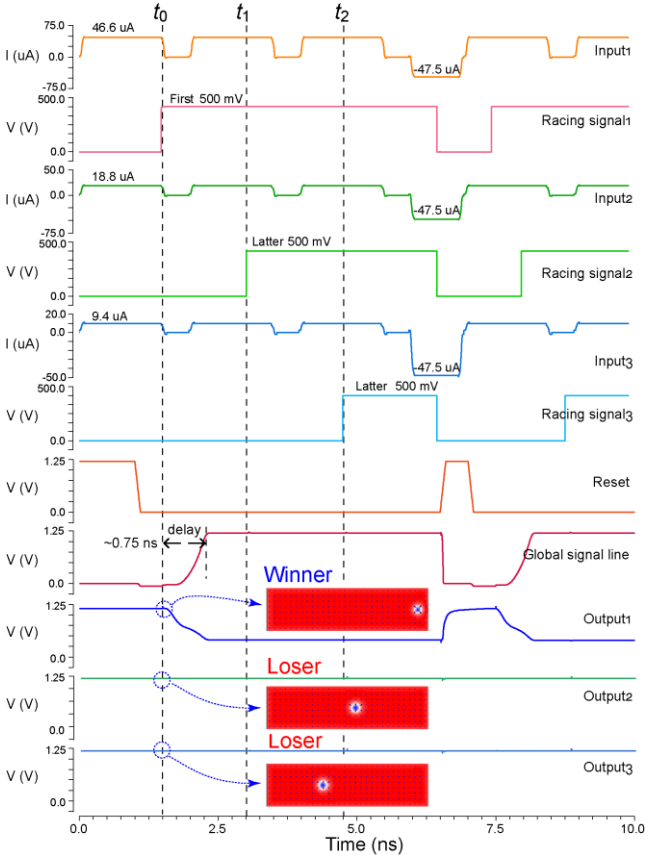


Fig. 6. Hybrid skyrmion/CMOS SPICE simulation waveforms of the proposed SR-WTA LIF spiking neuron network (three spike outputs as an example) under the 40 nm technology node.

racing velocity (or distance) as a function of the density (Fig. 5(a)) and frequency (Fig. 5(b)) of the input spiking current, respectively. In Fig. 5(a), we set a constant frequency of 500 MHz but vary the density (among 5 MA/cm<sup>2</sup>, 10 MA/cm<sup>2</sup>, and 15 MA/cm<sup>2</sup>) of the input spike current pulse. On the other hand, in Fig. 5(b), we set a constant amplitude of 5 MA/cm<sup>2</sup> but vary the frequency (500 MHz, 312.5 MHz, and 666.7 MHz) of the input spike current pulse. As can be seen, either the density or frequency should exceed a threshold to drive the skyrmion moving forward, i.e., integrate before “leaky” to the original position. The neuron associated with a high-intensity input-spike current will win over others. That is, if the amplitude or/and the frequency of the input spike current is large enough to overcome the gradually increased PMA energy (or repulsive force), the skyrmion moves forward; otherwise the skyrmion moves backward. Once the skyrmion reaches the finishing line under the detection unit (located at a pre-defined threshold distance), it will be detected via, e.g., the topological Hall effect or the magnetoresistance effect [13], and finally the neuron “fires” an output spike and then reset. The output spike signal is further propagated to the WTA module.

### B. SPICE Simulation

A SPICE electrical model of the LIF spiking neuron was developed in Verilog-A language. Hybrid skyrmion/CMOS SPICE simulations were performed under the 40 nm technology node to investigate the functionality and performance of the SR-WTA LIF spiking neuron network.

Fig. 6 shows the SPICE simulation waveforms with three neurons as an example, validating the functionality. Here the three input spike currents are with amplitudes of 46.6  $\mu$ A, 18.8  $\mu$ A, and 9.4  $\mu$ A, respectively, and with same pulse width of 1.5 ns. The skyrmion diameter is about 24 nm under the default parameters. Obviously, the neuron with the biggest input spike current first reaches the finishing line and wins over the others. Thanks to the high-speed and low-power current-induced skyrmion motion, the delay and energy of the proposed SR-WTA ILF spiking neuron network are rather small, about 0.75 ns and 0.65 mW in this example, which are much below conventional WTA circuits based on silicon integration. Furthermore, the resolution and capacity of the proposed SR-WTA ILF spiking neuron network is scalable and reconfigurable through tuning the nanotrack length or/and the intensity of the input spike current pulse.

## V. CONCLUSIONS

In this work, we proposed for the first time a time-domain SR-WTA network based on the LIF spiking neurons, which offers a single-device implementation of the neurons with compact area, high-speed and lower energy consumption. Based on micromagnetic and SPICE simulations, the functionality and performance of the SR-WTA LIF spiking neuron network were investigated. This preliminary result suggests new possibilities for utilization of SNN and will encourages us on promoting skyrmion-based devices in more complex neuromorphic applications

## REFERENCES

- [1] Y. Lecun, Y. Bengio, G. Hinton. Deep learning. *Nature*, vol. 521, no. 7553, pp. 436-444, 2015.
- [2] A. Sengupta, K. Roy. Encoding neural and synaptic functionalities in electron spin: a pathway to efficient neuromorphic computing. *Applied Physics Reviews* vol. 4, no. 4, pp. 1-23, 2017.
- [3] M. Prezioso, et al. 2015. Training and operation of an integrated neuromorphic network based on metal-oxide memristors. *Nature*, vol. 521, no. 7550, pp. 61-64, 2015.
- [4] L. Song, X. Qian, H. Li and Y. Chen. PipeLayer: a pipelined reram-based accelerator for deep learning, *International Symposium on High Performance Computer Architecture (HPCA)*, IEEE, Austin, TX, pp. 541-552, 2017.
- [5] P. Chi et al. PRIME: A Novel Processing-in-memory architecture for neural network computation in ReRAM-based main memory. *43rd Annual International Symposium on Computer Architecture (ISCA)*. Seoul, pp. 27-39, 2016.
- [6] A. Shafiee et al. ISAAC: a convolutional neural network accelerator with in-situ analog arithmetic in crossbars. *43rd Annual International Symposium on Computer Architecture (ISCA)*. ACM/IEEE, Seoul, pp. 14-26, 2016.
- [7] J. Grollier, D. Querlioz and M. D. Stiles, Spintronic nanodevices for bioinspired computing, *Proceedings of the IEEE*, vol. 104, no. 10, pp. 2024-2039, 2016.
- [8] B. Yu, D. Z. Pan, T. Matsunawa, and X. Zeng. Machine learning and pattern matching in physical design. *Asian and South Pacific Design Automation Conference (ASPDAC)*. IEEE/ACM, Japan, pp. 19-22, 2015.
- [9] I. Palit, et al. Analytically power and performance of a CNN system. *International Conference on Computer-Aided Design (ICCAD)*. IEEE/ACM, Austin, TX, pp. 186-193, 2015.
- [10] H. Markram, et al. Spike-timing-dependent plasticity: a comprehensive overview. United States: Frontiers Research Foundation, 2012.
- [11] X. Wu, V. Saxena, K. Zhu and S. Balagopal, A CMOS spiking neuron for brain-inspired neural networks with resistive synapses and in situ learning, *IEEE Trans. Circ. Syst. II: Expr. Briefs*, vol. 62, no. 11, pp. 1088-1092, 2015.
- [12] M. Chu, B. Kim, S. Park, H. Hwang, M. Jeon, B. H. Lee, B. -G. Lee, Neuromorphic hardware system for visual pattern recognition with memristor array and CMOS neuron, *IEEE Trans. Industrial Electron*, vol. 62, no. 4, pp. 2410-2419, 2015.
- [13] W. Kang, Y. Huang, X. Zhang, Y. Zhou and W. Zhao, Skyrmion Electronics: An Overview and Outlook, *Proceedings of the IEEE*, vol. 104, no. 10, pp. 2040-2061, 2016.
- [14] W. Kang et al., Compact Modeling and Evaluation of Magnetic Skyrmion-Based Racetrack Memory, *IEEE Transactions on Electron Devices*, vol. 64, no. 3, pp. 1060-1068, 2017
- [15] J. Sampaio, V. Cros, S. Rohart, A. Thiaville and A. Fert. Nucleation, stability and current-induced motion of isolated magnetic skyrmions nanostructures. *Nature Nanotechnology*, vol. 8, no. 11, pp. 839-844, 2013.
- [16] C. Moreau-Luchaire, et al. Additive interfacial chiral interaction in multilayers for stabilization of small individual skyrmions at room temperature," *Nat. Nanotechnol.*, vol. 11, no. 5, pp. 444-448, 2016.
- [17] G. Yu, et al. Room-temperature creation and spin-orbit torque manipulation of skyrmions in thin films with engineered asymmetry, *Nano Lett.*, vol. 6, no. 3, pp. 1981-1988, 2016.
- [18] W. Legrand, et al. Room-temperature current-induced generation and motion of sub-100 nm skyrmions, *Nano Lett.*, vol. 17, no. 4, pp. 2703-2712, 2017.
- [19] Y. Huang, W. Kang, X. Zhang, Y. Zhou, and W. Zhao, Magnetic skyrmion-based synaptic devices. *Nanotechnology*, vol. 28, no. 08LT02, pp. 1-7, 2016.
- [20] Z. He and D. Fan, A tunable magnetic skyrmion neuron cluster for energy efficient artificial neural network, *Design, Automation & Test in Europe Conference & Exhibition (DATE)*, Lausanne, pp. 350-355, 2017.
- [21] S. Li, W. Kang, Y. Huang, X. Zhang, Y. Zhou, and W. Zhao, Magnetic skyrmion-based artificial neuron device, *Nanotechnology*, vol. 28, no. 31LT01, pp.1-7, 2017.
- [22] M. Chu et al., Neuromorphic Hardware System for Visual Pattern Recognition with Memristor Array and CMOS Neuron, *IEEE Transactions on Industrial Electronics*, vol. 62, no. 4, pp. 2410-2419, 2015.
- [23] W. Jiang, et al. Direct observation of the skyrmion hall effect, *Nat. Phys.*, vol. 13, pp. 162-169, 2017.
- [24] X. Zhang, Y. Zhou, and M. Ezawa, Magnetic bilayer-skyrmions without skyrmion hall effect, *Nature Comm.*, vol. 7, no. 10293, pp. 1-7, 2016.
- [25] X. Chen, W. Kang et al. 2018. A compact skyrmionic leaky-integrate-fire spiking neuron device. *Nanoscale*, vol. 10, no. 13, pp. 6139-6146, 2018.
- [26] M. J. Donahue, and D. G. Porter, "OOMMF User's Guide," *Interagency Report NISTIR 6376*, Gaithersburg, 1999.
- [27] A. Hrabec, et al. Measuring and tailoring the Dzyaloshinskii-Moriya interaction in perpendicularly magnetized thin films, *Phys. Rev. B.*, vol. 90, no. 2, pp. 020402, 2014.